Pergamon

Int. J. Heat Mass Transfer. Vol. 37, No. 10, pp. 1475–1485, 1994

0017-9310/94 $7.00+0.00

0017-9310(93)E0096-Y

Mixed convection to power-law fluids from two-dimensional or axisymmetric bodies

D. L. MEISSNER,† D. R. JENG‡ and K. J. DE WITT§

†Owens-Illinois, Toledo, OH 43666, U.S.A.
‡Department of Mechanical Engineering, The University of Toledo, Toledo, OH 43606, U.S.A.
§Department of Chemical Engineering, The University of Toledo, Toledo, OH 43606, U.S.A.

(*Received* 11 *May* 1993 *and in final form* 17 *November* 1993)

Abstract—Momentum and heat transfer in mixed-convective, power-law fluid flow over arbitrarily shaped two-dimensional or axisymmetric bodies are examined theoretically. The Merk–Chao series expansion technique, with three mixed convection parameters, is used for the analysis. Solutions to the governing equations are obtained as universal functions which are independent of the geometry of the problem. Using the wall derivatives of these universal functions, results are given for the flow over the flat plate, the horizontal circular cylinder and the sphere. The results are compared with the literature for the limiting cases of forced and natural convection.

1. INTRODUCTION

THE BOUNDARY-LAYER transport phenomena in power-law non-Newtonian fluid flow has been investigated heavily since the initial work of Acrivos *et al.* [1] and Acrivos [2] in 1960. However, in most of this work it has been assumed that either forced or natural convection effects could be neglected. In practice it is sometimes found that both modes of convections are important. The present work was done to provide a theoretical means of analyzing the momentum and energy transport in such flows. The Merk–Chao series solution technique is used herein, so a brief history of the method seems appropriate.

An advance in the accuracy of boundary-layer series solutions was made possible by Merk [3] in 1959. He refined the 'wedge method' proposed by Meksyn [4] by choosing to treat the wedge parameter, Λ, as an independent variable rather than the streamwise coordinate, ξ. Thus, the Merk series were expanded about the local similarity solution rather than the forward stagnation point of the body, as had been the convention in the past. However, an error in the form of the series presented by Merk was found by independent researchers [5, 6]. Chao and Fagbenle [6] put forth a corrected form of Merk's series and used it to perform a universal, laminar boundary-layer analysis for the forced flow of Newtonian fluids over isothermal bodies. Since then, the 'Merk–Chao' approach has been used with success for a family of boundary-layer solutions. Some of the latest applications of the Merk–Chao series solution technique have been universal boundary-layer analyses of the mixed convection to Newtonian fluids [7] and the pure-forced [8] and pure-natural [9] convection to non-Newtonian power-law fluids.

In the present study, Merk–Chao series are used to perform a universal analysis of mixed convection in laminar boundary-layer flows of power-law fluids over arbitrarily shaped, smooth isothermal bodies. The three-parameter Merk–Chao series is developed herein, and is used to transform the governing partial differential equation set into a sequence of coupled ordinary differential equation sets, which govern the universal functions. Solutions have been obtained for combinations of the mixed-convection parameters for various combinations of n, the power-law exponent, and Pr, the general Prandtl number and are tabulated elsewhere [10]. Specific flow situations may be rapidly analyzed using these tabulated solutions or the computer programs in ref. [10]. Results of the application of the present method to flows over representative two-dimensional and axisymmetric bodies are presented in this paper.

2. PROBLEM FORMULATION

This treatment is for the steady, laminar, aiding, mixed-convective boundary-layer flow of a power-law fluid over a two-dimensional or axisymmetric body of arbitrary contour and uniform surface temperature, T_w, located in a mean flow of temperature T_∞. The flow situation is illustrated in Fig. 1. The coordinate x denotes the distance along the body surface from the forward stagnation point, and the coordinate y denotes the normal distance from the surface. Accordingly, the velocity components u and v are in the x- and y-directions, respectively. For axisymmetric flows, $r(x)$ represents the distance from the axis of symmetry to the body surface, and for two-dimensional flows, $r = L$, the reference length. Constant physical properties are assumed in the analysis, except for density in the buoyant-force term. Furthermore,

NOMENCLATURE

- C_f local friction factor
- C_{f1}, C_{f4}, C_{f7} C_f values for 1, 4 and 7 terms in the series expansion, respectively
- c_i coefficients in the Merk–Chao series ($c_0 = 1$)
- E variable in ref. [9] for Λ_E
- f dimensionless stream function
- f_i, θ_i universal functions in the Merk–Chao series
- Gr generalized Grashof number
- G_1–G_7 functions defined in equations (33)–(37)
- g, g_x gravitational acceleration, component of g in $-x$ direction
- K consistency index
- k thermal conductivity
- L reference length
- Nu local Nusselt number
- Nu_1, Nu_4, Nu_7 Nu values for 1, 4 and 7 terms in the series expansion, respectively
- n power-law exponent
- Pr generalized Prandtl number
- q_w local heat flux at the body surface
- Re generalized Reynolds number
- R_L convection ratio
- r normal distance from axis of symmetry to the body surface
- T temperature
- T_∞ temperature of the free stream
- T_w temperature of the body surface
- U pseudo-velocity function
- U_∞ fluid approach velocity
- U_R characteristic velocity for mixed convection
- u, v x- and y-direction velocity components, respectively
- u_a equivalent free-stream velocity function due to buoyancy
- u_e free-stream velocity function
- x, y coordinates along and normal to body surface, respectively.

Greek symbols

- α thermal diffusivity
- β coefficient of thermal expansion
- δ angle between flat plate and gravity vector
- $\delta_{2,i}$ Kronecker delta
- θ dimensionless temperature
- Λ_3, Λ_B, Λ_E mixed-convection parameters
- λ_r function defined in equation (38)
- ξ, η dimensionless coordinates along and normal to body surface, respectively
- ρ density
- τ_{yx} shear stress
- τ_w shear stress at the body surface
- ϕ dimensionless body coordinate, defined as x/L
- ψ stream function.

the viscous dissipation of energy and the y-momentum equation are neglected. Obviously, the results will lose accuracy as the y-component of gravity becomes comparable to the x-component for a situation where buoyant forces are comparable to the pressure forces. Note, however, that the main goal of this work was to apply a three-parameter series expansion technique to analyze mixed convection problems, and the application of this technique is unchanged by the inclusion of y-momentum effects.

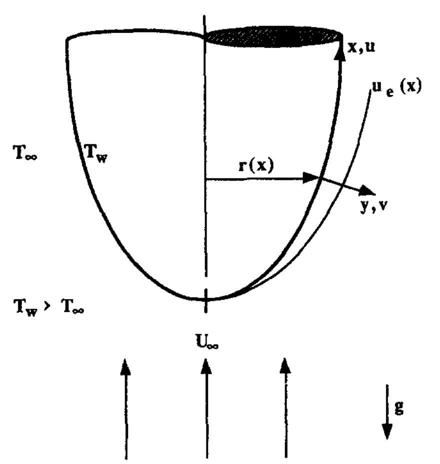

FIG. 1. Physical model and coordinate system.

The governing continuity, momentum and energy equations are:

$$\frac{\partial(ru)}{\partial x}+\frac{\partial(rv)}{\partial y}=0 \tag{1}$$

$$u\frac{\partial u}{\partial x}+v\frac{\partial u}{\partial y}=u_e\frac{du_e}{dx}+g_x\beta(T-T_\infty)+\frac{K}{\rho}\frac{\partial}{\partial y}\left[\frac{\partial u}{\partial y}\left|\frac{\partial u}{\partial y}\right|^{n-1}\right] \tag{2}$$

$$u\frac{\partial T}{\partial x}+v\frac{\partial T}{\partial y}=\alpha\frac{\partial^2 T}{\partial y^2} \tag{3}$$

with the boundary conditions:

$$\begin{aligned} &@\ y=0 \quad && u=v=0 \quad && T=T_w \\ &@\ x=0 \quad && u=u_e(0) \quad && T=T_\infty \\ &@\ y\to\infty \quad && u\to u_e(x) \quad && T\to T_\infty \end{aligned} \tag{4}$$

where $u_e(x)$ is the velocity at the outer edge of the boundary layer. It is assumed to be known from either experiment or inviscid flow theory. For the power-law model, the shear stress can be expressed as:

$$\tau_{yx} = K\left|\frac{\partial u}{\partial y}\right|^{n-1}\frac{\partial u}{\partial y} \tag{5}$$

where n is the positive-valued, dimensionless power-law exponent and K is the non-Newtonian consistency index, whose units obviously depend on the value of n.

3. SOLUTION PROCEDURE

Since there are only two velocity components, a stream function $\psi(x, y)$ can be used to automatically satisfy continuity by letting:

$$u = \frac{1}{r}\frac{\partial\psi}{\partial y} \quad \mathrm{v} = -\frac{1}{r}\frac{\partial\psi}{\partial x} \tag{6}$$

and the number of equations to be solved is reduced to two.

As done by Cameron *et al.* [7], a pseudo-velocity function, $U(x)$, is defined as:

$$U\frac{\mathrm{d}U}{\mathrm{d}x} = u_e\frac{\mathrm{d}u_e}{\mathrm{d}x} + g_x\beta(T_w - T_\infty) = u_e\frac{\mathrm{d}u_e}{\mathrm{d}x} + u_a\frac{\mathrm{d}u_a}{\mathrm{d}x} \tag{7}$$

and the mixed-convection reference velocity as:

$$U_R = U_\infty + [g\beta L(T_w - T_\infty)]^{1/2}. \tag{8}$$

The generalized Reynolds, Prandtl and Grashof numbers are defined as usual for power-law fluids, while using U_R as the characteristic velocity in Re and Pr.

$$Re = \frac{\rho U_R^{2-n}L^n}{K} \quad Pr = \frac{1}{\alpha}\left(\frac{K}{\rho}\right)^{2/(n+1)}\left(\frac{U_R^3}{L}\right)^{(n-1)/(n+1)}$$

$$Gr = \frac{\rho^2 L^{n+2}[g\beta(T_w - T_\infty)]^{2-n}}{K^2}. \tag{9}$$

The results presented herein are in terms of Re, but for pure-free convection the relation $Re = \sqrt{Gr}$ can be used to put them in terms of Gr.

The x, y coordinate system is transformed into a dimensionless system by adopting the dimensionless variables:

$$\xi(x) = \frac{n}{Re}\int_0^x\left(\frac{U}{U_R}\right)^{2n-1}\left(\frac{r}{L}\right)^{n+1}\left(\frac{\mathrm{d}x}{L}\right) \tag{10}$$

$$\eta(x, y) = \left[\frac{1}{(n+1)\xi}\right]^{1/(n+1)}\left(\frac{Ury}{U_R L^2}\right). \tag{11}$$

Also, the dimensionless stream function, $f(\xi, \eta)$, and temperature, $\theta(\xi, \eta)$, are given respectively as:

$$\psi(x, y) = [(n+1)\xi]^{1/(n+1)}U_R L^2 f(\xi, \eta) \tag{12}$$

$$\theta(\xi, \eta) = \frac{T(x, y) - T_\infty}{T_w - T_\infty}. \tag{13}$$

By substituting equations (6), (10)–(13) into equations (2) and (3), the following equation set is obtained:

$$f'''|f''|^{n-1} + ff'' - \Lambda_3(f')^2 + \Lambda_3(1-\Lambda_B^2)\theta + \Lambda_3\Lambda_B^2 = (n+1)\xi\left[\frac{\partial(f', f)}{\partial(\xi, \eta)} + \Lambda_B\frac{\mathrm{d}\Lambda_B}{\mathrm{d}\xi}(\theta - 1)\right] \tag{14}$$

$$\theta'' + \frac{nPr}{\Lambda_E}(f\theta') = \frac{nPr}{\Lambda_E}\left[(n+1)\xi\frac{\partial(\theta, f)}{\partial(\xi, \eta)}\right] \tag{15}$$

with the corresponding boundary conditions:

$$f(\xi, 0) = f'(\xi, 0) = 0 \quad f'(\xi, \eta\to\infty)\to\Lambda_B$$
$$\theta(\xi, 0) = 1 \quad \theta(\xi, \eta\to\infty)\to 0 \tag{16}$$

where the primes denote differentiation with respect to η, and $\partial(\ ,\ )/\partial(\xi, \eta)$ denotes the Jacobian. The Λs are the mixed-convection parameters defined as:

$$\Lambda_3 = (n+1)\xi\frac{1}{U}\frac{\mathrm{d}U}{\mathrm{d}\xi} \qquad \Lambda_B = \frac{u_e}{U}$$

$$\Lambda_E = \left[\frac{n(n+1)\xi U_R^3}{\frac{\mathrm{d}\xi}{\mathrm{d}\phi}U^3}\right]^{(n-1)/(n+1)} \tag{17}$$

with $\phi = x/L$.

The idea of expanding the dimensionless stream function and temperature into series is that of eliminating all explicit ξ dependence from the formulation. The use of Merk–Chao series results in solutions which are perturbed about a local similarity state. For this reason, the accuracy is expected to be good throughout the entire range of all the parameters involved.

For most previous applications of the Merk-type series approach, only one ξ-dependent parameter has appeared in the transformed equations, and, correspondingly, only the perturbations arising due to the local variation in that quantity were accounted for in the series. In the analysis of mixed convection to Newtonian fluids [7], two independent ξ-dependent parameters, Λ_3 and Λ_B, arose in the transformed equations, and Cameron *et al.* [7] used two-parameter Merk–Chao series. In the present work, a third parameter, Λ_E, which is characteristic of power-law fluids, is present in the transformed energy equation. Although it may be possible to express this parameter explicitly in terms of Λ_3 and Λ_B, no such expression was found. If this function was found, it would eliminate the need for the three-parameter series expansions used herein. The three-parameter Merk–Chao series employed for the dimensionless stream function is:

$$f = f_0 + (n+1)\xi \frac{d\Lambda_3}{d\xi} f_1 + (n+1)\xi \frac{d\Lambda_B}{d\xi} f_2 + (n+1)\xi \frac{d\Lambda_E}{d\xi} f_3 + [(n+1)\xi]^2 \frac{d^2\Lambda_3}{d\xi^2} f_4 + [(n+1)\xi]^2 \frac{d^2\Lambda_B}{d\xi^2} f_5 + [(n+1)\xi]^2 \frac{d^2\Lambda_E}{d\xi^2} f_6 + \left[(n+1)\xi \frac{d\Lambda_3}{d\xi}\right]^2 f_7 + \left[(n+1)\xi \frac{d\Lambda_B}{d\xi}\right]^2 f_8 + \left[(n+1)\xi \frac{d\Lambda_E}{d\xi}\right]^2 f_9 + [(n+1)\xi]^2 \frac{d\Lambda_3}{d\xi}\frac{d\Lambda_B}{d\xi} f_{10} + [(n+1)\xi]^2 \frac{d\Lambda_3}{d\xi}\frac{d\Lambda_E}{d\xi} f_{11} + [(n+1)\xi]^2 \frac{d\Lambda_B}{d\xi}\frac{d\Lambda_E}{d\xi} f_{12} + \cdots \quad (18)$$

where $f_i = f_i(\Lambda_3, \Lambda_B, \Lambda_E, n, Pr, \eta)$ are the universal functions for the dimensionless stream function. An identical expansion is also used to express the dimensionless temperature in terms of the universal functions for dimensionless temperature, $\theta_i = \theta_i(\Lambda_3, \Lambda_B, \Lambda_E, n, Pr, \eta)$. Before the results of the series substitutions are given, there is one detail of the development which is worthy of note. The term $|f''|^{n-1}$ which appears in equation (14) must be dealt with carefully. If the value of f'' is expected to be negative at any location in the flow field, which will occur if the u-velocity profile reaches a maximum anywhere inside the momentum boundary layer, then it is necessary to make the assumption:

$$f'' \approx f_0'' \Rightarrow |f''|^{n-1} \approx |f_0''|^{n-1} \quad (19)$$

as was done by Chang *et al.* [9]. However, if f'' is expected to be everywhere positive, the absolute value signs can be dropped, and the quantity can be represented more accurately by including the second term of the binomial series. That is:

$$(f'')^{n-1} = \left(\sum_{i=0}^{\text{terms}-1} c_i f_i''\right)^{n-1} \approx (f_0'')^{n-1} + (n-1)(f_0'')^{n-2} \sum_{i=1}^{\text{terms}-1} c_i f_i'' \quad (20)$$

where c_i represents the series coefficient of f_i, with $c_0 = 1$. Again, the physical interpretation of when the extra terms may be used is for any case where the buoyancy effects are small enough that the u-velocity profile never reaches a maximum inside the momentum boundary layer. In the equations below, the terms which arise due to the use of approximation (20), rather than (19), are denoted with an asterisk (*).

Substituting equation (18) and the dimensionless temperature counterpart into equations (14) and (15), neglecting all squared-derivative, cross-derivative and third-or-higher-order derivative terms ($i > 6$ terms) and collecting terms with common series coefficients results in the first seven ordinary differential equation sets which govern the universal functions. The similarity equation set, which is the only nonlinear set, is:

$$f_0''' + [f_0 f_0'' - \Lambda_3 (f_0')^2 + \Lambda_3 (1-\Lambda_B^2)\theta_0 + \Lambda_3 \Lambda_B^2] |f_0''|^{1-n} = 0 \quad (21)$$

$$\theta_0'' + \frac{n\,Pr}{\Lambda_E}(f_0 \theta_0') = 0 \quad (22)$$

with boundary conditions:

$$f_0(\xi,0) = f_0'(\xi,0) = 0 \quad f_0'(\xi,\eta\to\infty)\to\Lambda_B$$
$$\theta_0(\xi,0) = 1 \quad \theta_0(\xi,\eta\to\infty)\to 0. \quad (23)$$

The first-order perturbation ($i = 1$–3) equation sets are given by:

$$f_i''' + [f_0 f_i'' - (2\Lambda_3 + n + 1) f_0' f_i' + (n+2) f_0'' f_i + \Lambda_3(1-\Lambda_B^2)\theta_i] |f_0''|^{1-n} + {}^*(1-n) f_0''' (f_0'')^{-1} f_i'' = \left[\frac{\partial(f_0', f_0)}{\partial(\Lambda_i, \eta)} + \delta_{2,i}\Lambda_B(\theta_0 - 1)\right] |f_0''|^{1-n} \quad (24)$$

$$\theta_i'' + \frac{n\,Pr}{\Lambda_E}[f_0\theta_i' - (n+1) f_0'\theta_i + (n+2)\theta_0' f_i] = \frac{n\,Pr}{\Lambda_E}\left[\frac{\partial(\theta_0, f_0)}{\partial(\Lambda_i, \eta)}\right] \quad (25)$$

where $\Lambda_i = \Lambda_3, \Lambda_B, \Lambda_E$ for $i = 1, 2, 3$ and $\delta_{2,i}$ is the Kronecker delta. The second-order perturbation equation sets ($i = 4$–6) are:

$$f_i''' + [f_0 f_i'' - 2(\Lambda_3 + n + 1) f_0' f_i' + (2n+3) f_0'' f_i + \Lambda_3(1-\Lambda_B^2)\theta_i] |f_0''|^{1-n} + {}^*(1-n) f_0''' (f_0'')^{-1} f_i'' = (f_0' f_{i-3}' - f_0'' f_{i-3}) |f_0''|^{1-n} \quad (26)$$

$$\theta_i'' + \frac{n\,Pr}{\Lambda_E}[f_0\theta_i' - 2(n+1) f_0'\theta_i + (2n+3)\theta_0' f_i] = \frac{n\,Pr}{\Lambda_E}(f_0'\theta_{i-3} - \theta_0' f_{i-3}) \quad (27)$$

with the corresponding boundary conditions ($i =$ 1–6):

$$f_i(\xi,0) = f_i'(\xi,0) = 0 \quad f_i'(\xi,\eta\to\infty)\to 0$$
$$\theta_i(\xi,0) = 0 \quad \theta_i(\xi,\eta\to\infty)\to 0. \quad (28)$$

As pointed out by Acrivos *et al.* [1], to allow solutions for $n \geqslant 2$ the free-stream conditions for f_i' in (23) and (28) must be applied at a finite η, rather than at infinity, due to the mathematical nature of the momentum equations in the free stream.

It seems appropriate at this point to discuss how equations (21)–(28) relate to the analogous equations in the literature for various limiting cases. First, the work that constitutes the limiting case of this study for Newtonian fluids is that of Cameron *et al.* [7], and our analysis reduces identically to that in ref. [7] for $n = 1$. As is clear from equation (17), for Newtonian fluid flows, $\Lambda_E = 1$, and the $i = 3$ and 6 terms disappear from the Merk–Chao series. The analysis most closely related to the present for pure-forced convection to power-law fluids is that in ref. [8]. For this case, $\Lambda_B = 1$, which allows the momentum analysis to proceed independent of energy transport considerations. The momentum analysis in ref. [8] is identical to that herein and involves only the similarity ($i = 0$) and Λ_3-related ($i = 1$ and 4) perturbation equations, with the * terms included. However, Kim *et al.* [8] used completely different series substitutions to perform their energy analysis for a step-change surface temperature distribution. The isothermal surface is the limiting case, for which the largest error in their series solution is to be expected. Chang *et al.* [9] obtained the analogous pure-natural convection ($\Lambda_B = 0$) solution for power-law fluid flow over an isothermal surface by using Merk-type series for both the dimensionless stream function and temperature. The only differences between the present analysis and that in ref. [9] are that in the latter no results were obtained for dilatant fluids ($n > 1$), possibly due to the singularity encountered in equation (21) for such fluids when the f_0' profile reaches a maximum, and that the Λ_E (called E, the energy parameter, in ref. [9])-related terms were not included in their series expansions. Thus, the equations governing the universal functions in ref. [9] are obtained by setting $\Lambda_B = 0$ in equations (21)–(28) and, as for forced convection, using only the similarity and $i = 1$ and 4 perturbation equations, but with the * terms left out. Incidentally, for the results obtained in this study, it was found that the Λ_E-related terms contributed only minimally (about 3% at most) to the Nusselt number group for $\Lambda_B = 0$, and hence the deviation of our results from those of Chang *et al.* [9] is small.

The equation sets governing the universal functions were solved sequentially for the universal wall derivatives, $f_i''(\Lambda_3, \Lambda_B, \Lambda_E, n, Pr, \eta = 0)$ and $\theta_i'(\Lambda_3, \Lambda_B, \Lambda_E, n, Pr, \eta = 0)$, using the fourth-order Runge–Kutta method with an automatic, interval-halving-based step-size adjustment. Equations (21)–(23) were solved using the shooting method, and equations (24)–(28) were solved using superposition. A Cray-XMP2/8 computer was used, due to the large number of parameter variations solved for in ref. [10]. The details of the solution procedure can be found in ref. [10], where results are tabulated for Λ_B ranging from 0.0 to 1.0 and Λ_3 and Λ_E ranging from 0.5 to 1.0 for fifteen different combinations of n and Pr. The n values ranged from 0.5 to 2.0 and the Pr values from 1.0 to 100. The full results from ref. [10] are available on floppy disk from the authors. For the convenience of the reader, the universal wall derivatives for the $n = 1.6$, $Pr = 100$ combination are given here in Table 1, with the corresponding case definitions in Table 2. This n, Pr combination is the one used in generating the results for specific geometries, which are presented in the following section. The asterisks (*) in Table 1 denote the cases for which the * terms in equations (24) and (26) were left in. The computational times for the results presented herein averaged approximately 5 CPU seconds per parameter set.

In all instances, we were able to reproduce the results of Cameron *et al.* [7]; this was used as a check of our computer programs. Also, our wall derivatives of the similarity solution universal functions generally matched those in refs. [8, 9] (f_0'' in ref. [8] and f_0'' and θ_0' in ref. [9]) to at least four significant figures. There was at most a 0.5% difference between our wall derivatives of the perturbation universal functions and those in refs. [8, 9] (f_i'' in ref. [8] and f_i'' and θ_i' in ref. [9], for $i = 1$ and 4). These differences are due to slight differences in the numerical solution techniques, not actual differences in the equations, since our equations reduce appropriately to match those in refs. [7–9].

4. APPLICATION TO SPECIFIC GEOMETRIES

First, a parameter must be defined to characterize the mixed-convection situation. The convention of Cameron *et al.* [7] is adopted in defining the convection ratio as:

$$R_L = \frac{U_\infty}{U_\infty + [g\beta L(T_w - T_\infty)]^{1/2}}. \tag{29}$$

Generally, the quantities of interest are the local shear stress and heat flux at the body surface. These are defined as usual:

$$\tau_w = K\left(\frac{\partial u}{\partial y}\right)^n\bigg|_{y=0} \quad q_w = -k\frac{\partial T}{\partial y}\bigg|_{y=0}. \tag{30}$$

The dimensionless forms of these quantities are the friction factor and Nusselt number:

$$\tfrac{1}{2}C_f = \frac{\tau_w}{\rho U_R^2} \quad Nu = \frac{q_w L}{k(T_w - T_\infty)}. \tag{31}$$

The results are independent of the Reynolds number if the following groupings, called the friction factor and Nusselt number groups herein, are used:

$$\tfrac{1}{2}C_f\, Re^{1/(n+1)} \quad Nu\, Re^{-1/(n+1)}. \tag{32}$$

However, for a general mixed-convection analysis, it is not possible to absorb the Prandtl number dependence into these groups.

To define a specific flow situation, one must specify constant values for n, Pr and R_L and also dimensionless forms of $u_e(x)$, $u_a(x)$ and $r(x)$. Using these, one obtains values for the three Λ parameters, the Merk–Chao series coefficients and the friction factor and Nusselt number group coefficients for selected locations on the body surface. The development of these expressions is as follows:

$$u_e = U_\infty G_1(\phi) \quad u_a = \sqrt{(g\beta L(T_w - T_\infty))}\, G_2(\phi). \tag{33}$$

Table 1. Wall derivatives of universal functions; $n = 1.60$, $Pr = 100$

Case	f_0''	$f_1''\times 10$	$f_2''\times 10$	$f_3''\times 10$	$f_4''\times 10^2$	$f_5''\times 10^2$	$f_6''\times 10^2$
1	0.33137107	−0.154	−0.233	−0.512	0.216	0.328	0.807
*2	0.39372314	−0.083	1.732	−0.225	0.093	−0.775	0.340
*3	0.56321306	−0.128	3.309	−0.129	0.114	−1.525	0.194
*4	0.79349227	−0.195	4.170	−0.055	0.159	−1.903	0.082
*5	1.05608720	−0.271	4.675	−0.000	0.213	−2.109	0.000
6	0.37051970	−0.179	−0.249	−0.279	0.245	0.352	0.441
*7	0.42656390	−0.095	1.449	−0.129	0.105	−0.657	0.196
*8	0.58281211	−0.132	2.948	−0.077	0.119	−1.426	0.116
*9	0.80199228	−0.196	3.846	−0.034	0.161	−1.848	0.050
*10	1.05608720	−0.271	4.386	−0.000	0.213	−2.083	0.000
11	0.47335332	−0.102	−0.177	−0.721	0.144	0.242	1.132
*12	0.53879889	−0.053	1.091	−0.328	0.062	−0.314	0.495
*13	0.72790978	−0.071	2.270	−0.198	0.060	−0.792	0.298
*14	0.99565399	−0.102	2.989	−0.087	0.072	−1.072	0.130
*15	1.30747286	−0.138	3.419	−0.000	0.089	−1.229	0.000
16	0.52880794	−0.116	−0.188	−0.391	0.160	0.257	0.615
*17	0.58662761	−0.060	0.899	−0.186	0.070	−0.248	0.282
*18	0.75786830	−0.074	1.991	−0.117	0.064	−0.723	0.176
*19	1.00903812	−0.103	2.728	−0.053	0.073	−1.032	0.079
*20	1.30747286	−0.138	3.189	−0.000	0.089	−1.212	0.000
	θ_0'	$\theta_1'\times 10$	$\theta_2'\times 10$	$\theta_3'\times 10$	$\theta_4'\times 10^2$	$\theta_5'\times 10^2$	$\theta_6'\times 10^2$
1	−2.59184398	−0.470	1.264	−2.707	0.825	−1.655	4.037
*2	−2.88128293	−0.740	−9.444	−4.383	1.211	6.204	6.606
*3	−3.37250403	−0.579	−12.116	−5.413	1.092	6.749	8.106
*4	−3.83741088	−0.504	−11.439	−6.268	1.079	5.931	9.360
*5	−4.24760666	−0.484	−10.336	−6.982	1.121	5.171	10.415
6	−2.12551121	−0.353	1.029	−1.143	0.658	−1.338	1.698
*7	−2.32971453	−0.603	−6.117	−1.764	0.996	4.262	2.658
*8	−2.68926410	−0.480	−8.590	−2.155	0.891	5.135	3.229
*9	−3.04341235	−0.407	−8.446	−2.490	0.860	4.673	3.718
*10	−3.36152286	−0.380	−7.777	−2.772	0.878	4.130	4.134
11	−2.91711507	−0.296	0.762	−3.082	0.502	−0.962	4.623
*12	−3.16946277	−0.456	−5.573	−4.798	0.734	3.853	7.241
*13	−3.64373058	−0.409	−8.040	−5.840	0.723	4.794	8.752
*14	−4.11713684	−0.387	−7.977	−6.739	0.746	4.435	10.065
*15	−4.54467454	−0.389	−7.363	−7.498	0.789	3.951	11.183
16	−2.39101633	−0.233	0.618	−1.304	0.410	−0.774	1.951
*17	−2.56614417	−0.370	−3.538	−1.937	0.600	2.571	2.922
*18	−2.90744777	−0.334	−5.623	−2.328	0.586	3.578	3.491
*19	−3.26388139	−0.311	−5.854	−2.678	0.594	3.454	4.000
*20	−3.59293212	−0.306	−5.531	−2.977	0.620	3.133	4.439

Using the definitions of R_L and U_R, and the fact that $U = \sqrt{(u_e^2+u_a^2)}$, we see that:

$$U = U_R\sqrt{(R_L^2G_1^2+(1-R_L)^2G_2^2)} = U_RG_3(\phi). \quad (34)$$

Thus,

$$\frac{dU}{d\phi} = U_R\frac{\left[\dfrac{1}{2}\dfrac{dG_3^2}{d\phi}\right]}{G_3} = U_R\frac{G_4(\phi)}{G_3}. \quad (35)$$

For axisymmetric flows the functions

$$r = LG_5(\phi) \qquad \frac{dr}{d\phi} = LG_6(\phi) \quad (36)$$

are needed, and for two-dimensional flows $G_5 = 1$ and $G_6 = 0$. Also, the operator

$$\xi\frac{d}{d\xi} = \left(\frac{\int_0^\phi G_3^{2n-1}G_5^{n+1}\,d\phi}{G_3^{2n-1}G_5^{n+1}}\right)\frac{d}{d\phi} = G_7(\phi,n)\frac{d}{d\phi} \quad (37)$$

is needed. Now, all of the flow-situation-dependent quantities are expressed in terms of the above G functions as follows:

$$\Lambda_3 = \frac{(n+1)\,G_7\,G_4}{G_3^2} \qquad \Lambda_B = \frac{R_L\,G_1}{G_3}$$

$$\Lambda_E = \left[\frac{n(n+1)\,G_7}{G_3^3}\right]^{(n-1)/(n+1)} \qquad \lambda_r = \frac{(n+1)\,G_7\,G_6}{G_5} \quad (38)$$

Table 2. Case definitions

Λ_B	0.00	0.25	0.50	0.75	1.00
$\Lambda_3 = 0.50$, $\Lambda_E = 0.50$	1	2	3	4	5
$\Lambda_3 = 0.50$, $\Lambda_E = 1.00$	6	7	8	9	10
$\Lambda_3 = 1.00$, $\Lambda_E = 0.50$	11	12	13	14	15
$\Lambda_3 = 1.00$, $\Lambda_E = 1.00$	16	17	18	19	20

where λ_r, which is defined as $(n+1)\xi(1/r)(dr/d\xi)$, is used below in equation (40). The Merk–Chao series coefficients for $i = 1$–3 are given by:

$$c_i = (n+1)\xi\frac{d\Lambda}{d\xi} = (n+1)G_7\frac{d\Lambda}{d\phi} \tag{39}$$

and for $i = 4$–6 by:

$$c_i = [(n+1)\xi]^2\frac{d^2\Lambda}{d\xi^2} = [(n+1)G_7]^2\frac{d^2\Lambda}{d\phi^2} + (n+1)\xi\frac{d\Lambda}{d\xi}[(1-2n)\Lambda_3-(n+1)\lambda_r] \tag{40}$$

where the derivatives of the Λs with respect to ϕ in equations (39) and (40) can be evaluated analytically or numerically. Lastly, the friction factor and Nusselt number group coefficients, given in terms of the G functions, are defined by:

$$\tfrac{1}{2}C_f\,Re^{1/(n+1)} = \left[\frac{G_3^3}{n(n+1)G_7}\right]^{n/(n+1)}[f''(\eta=0)]^n \tag{41}$$

$$Nu\,Re^{-1/(n+1)} = -\left[\frac{G_3^{2-n}}{n(n+1)G_7}\right]^{1/(n+1)}\theta'(\eta=0) \tag{42}$$

where

$$f''(\eta=0) = \sum_{i=0}^{6} c_i f_i''(\eta=0)$$

$$\theta'(\eta=0) = \sum_{i=0}^{6} c_i\theta_i'(\eta=0). \tag{43}$$

Note that the generalized Prandtl number was not needed in developing equations (33)–(42). In fact, the explicit existence of Pr in the formulation could have been eliminated by scaling Λ_E by $1/Pr$, but this was decided against.

For each position along the body, the corresponding Λ_3, Λ_B and Λ_E, along with n and Pr, are used to obtain $f_i''(\eta=0)$ and $\theta_i'(\eta=0)$ for (43) by using the computer programs or the tables in ref. [10].

Now results are given from the analysis of some common geometries. For all of these results, the combination $n = 1.60$, $Pr = 100$ was chosen for presentation. This was because ref. [9], which represents a limiting case of this analysis, did not include any results for $n > 1$, and because power-law fluids typically have high Prandtl numbers. For each geometry, solutions were generated for five values of the convection ratio, R_L, which represent pure-natural convection ($R_L = 0.00$), pure-forced convection ($R_L = 1.00$) and three combinations thereof ($R_L =$ 0.25, 0.50 and 0.75).

4.1. *Flat plate*

The first geometry studied was the flat plate. With U_R defined as in equation (8), the analysis is for a vertical plate, and if the g in equation (8) is replaced by g cos (δ), where δ is the angle between the plate and the gravity vector, the results apply to an inclined plate as well, until, of course, the y-direction buoyant forces become important. For this geometry, the three defining functions are simply:

$$G_1 = 1 \quad G_2 = \sqrt{(2\phi)} \quad G_5 = 1. \tag{44}$$

For all values of R_L, Λ_3 is a constant over the plate length, and for $R_L = 0.0$ or 1.0, Λ_B is also constant. Thus, for pure-free or pure-forced convection, only the Λ_E-related ($i = 3$ and 6) perturbation terms are active, which creates a good opportunity to observe their effect on the overall results. Table 3 illustrates the relative convergence of the Merk–Chao series for the flat plate through the ratios of the one- and four-term friction factor and Nusselt number groups to the corresponding seven-term groups. The effect of the Λ_E-related terms on the Nusselt number group was about 6% for pure-forced convection and decreased with decreasing R_L to a contribution of only about 1% for pure-free convection. As for the friction factor group, the Λ_E-related terms contributed 1% or less, except for the 2.4% for $R_L = 0.0$, but for natural convection flows friction factor information is usually of secondary importance. Table 3 also shows that, for mixed convection for the plate, retaining the series correction terms is vital to obtain accurate results, owing mainly to the importance of the Λ_B-related perturbation terms.

Figure 2 contains the friction factor group curves. For $R_L = 1.0$, our curve agrees exactly with the result of Kim *et al.* [8] and agrees with the result of Acrivos *et al.* [1] to within the accuracy that their value could be read from their figure. The high-Prandtl-number asymptotic solutions of Acrivos *et al.* [1] ($R_L = 1.0$) and Acrivos [2] ($R_L = 0.0$) are plotted in Fig. 3 along with our Nusselt number group curves. The forced convection results differ consistently by about 5% over the entire length of the plate, and the free convection results differ by between 2.0 and 2.8% over the length, with our Nusselt number groups being the lower in both cases.

4.2. *Horizontal circular cylinder*

The next geometry considered was the infinite, horizontal cylinder in crossflow, for which the choice of the G_1 function is very important. For bluff bodies like the cylinder (or the sphere, which is considered next), separation of the boundary layer causes a broad wake which alters the free-stream velocity behavior. In such cases, the use of the Potential Flow Theory to predict $u_e(x)$, rather than an experimental pressure distribution, is well known to cause severe errors in boundary-layer results. The experimental pressure distribution of Shah *et al.* [11], given below in (45), was used in this work to effect a direct comparison with ref. [8]. The expression in ref. [11] was obtained by fitting data from various pseudoplastic fluids for

Table 3. Relative convergence of the Merk–Chao series as applied to the flat plate; $n = 1.60$, $Pr = 100$

ϕ	R_L	C_{f1}/C_{f7}	C_{f4}/C_{f7}	Nu_1/Nu_7	Nu_4/Nu_7
0.05	1.00	1.000	1.000	0.940	0.986
1.00	1.00	1.000	1.000	0.940	0.986
0.05	0.75	1.528	1.065	1.187	1.032
1.00	0.75	1.491	1.061	1.180	1.031
0.05	0.50	1.534	1.065	1.188	1.032
1.00	0.50	1.320	1.039	1.142	1.026
0.05	0.25	1.426	1.052	1.167	1.029
1.00	0.25	1.052	1.004	1.052	1.011
0.05	0.00	0.976	0.993	1.011	1.003
1.00	0.00	0.976	0.993	1.011	1.003

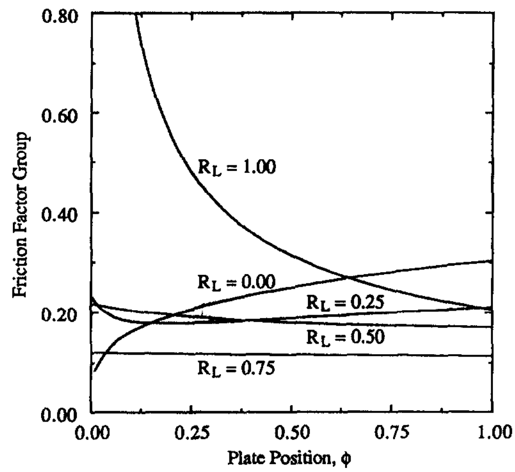

FIG. 2. Local friction factor group curves for the inclined plate; $n = 1.6$, $Pr = 100$.

cylinder angles ranging from 0 to 60° from the forward stagnation point. It does not provide an adverse pressure gradient until after the known separation point of around 80°, so prediction of a realistic separation point was not possible. The pertinent G functions for the horizontal cylinder are:

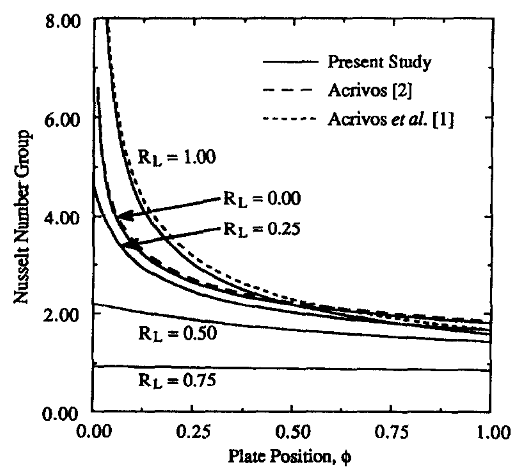

FIG. 3. Local Nusselt number group curves for the inclined plate and comparison with refs. [1, 2]; $n = 1.6$, $Pr = 100$.

$$G_1 = 1.84\phi - 0.262\phi^3$$

$$G_2 = \sqrt{(2(1-\cos\phi))} \quad G_5 = 1. \tag{45}$$

Table 4 shows the relative convergence of the Merk–Chao series for the horizontal cylinder results. The series convergence is seen to be very good, with the similarity-solution groups being within 6.4 and 6.1% of the corresponding seven-term-series groups for the friction factor and Nusselt number groups, respectively, for all of the cases tabulated. However, for large values of R_L and angles nearing the adverse pressure gradient, the series become semi-divergent and more terms appear to be needed. This phenomenon is more apparent in the sphere results below (Table 5).

Figures 4 and 5, respectively, show the friction factor and Nusselt number group curves. For $R_L = 1.0$, our friction factor group curve matches that in ref. [8] with a maximum difference of 0.8%, the discrepancy again being due only to numerical solution details. As shown in Fig. 5, the Nusselt number group curve of Kim *et al.* [8] is between 2.0 and 4.3% higher than the results of the present study, and the latter should be regarded as the more accurate solution since, for the energy analysis in ref. [8], the isothermal surface condition introduces the largest error in the series solution. Also, it should be mentioned that in ref. [8] the reference velocity used was twice the reference velocity used in our work, which meant that different Prandtl numbers had to be used to allow a comparison. To achieve this, the results in ref. [8] for $Pr = 100$ were extrapolated out to the comparable Pr ($100 \cdot 2^{(3n-3)/(n+1)} = 161.59$) using the well-known fact that Nu is proportional to $Pr^{1/3}$ for high Pr and forced flow. The accuracy of the comparison was then verified by using the G_1 from ref. [8] ($0.92\phi - 0.131\phi^3$) and comparing directly with the results in ref. [8]. For $R_L = 0.0$, our Nusselt number curve agrees everywhere within 1.6% with the asymptotic solution of Acrivos [2], except very near the stagnation point ($\phi < 3°$).

4.3. *Sphere*

Solutions were also generated for the sphere to illustrate the application of the present method to an axi-

Table 4. Relative convergence of the Merk–Chao series as applied to the horizontal cylinder; $n = 1.60$, $Pr = 100$

ϕ (deg)	R_L	C_{f1}/C_{f7}	C_{f4}/C_{f7}	Nu_1/Nu_7	Nu_4/Nu_7
5	1.00	1.000	1.000	1.048	1.015
60	1.00	0.982	1.002	1.028	1.011
75	1.00	0.936	1.066	1.012	1.004
5	0.75	0.999	1.000	1.048	1.015
60	0.75	0.989	1.001	1.030	1.011
75	0.75	0.959	1.017	1.020	1.005
5	0.50	0.998	1.000	1.048	1.015
60	0.50	1.023	1.000	1.045	1.012
75	0.50	1.054	0.999	1.055	1.008
5	0.25	0.987	0.996	1.046	1.014
60	0.25	1.034	0.997	1.061	1.013
5	0.00	0.940	0.984	1.033	1.010
60	0.00	0.941	0.981	1.028	1.009

Table 5. Relative convergence of the Merk–Chao series as applied to the sphere; $n = 1.60$, $Pr = 100$

ϕ (deg)	R_L	C_{f1}/C_{f7}	C_{f4}/C_{f7}	Nu_1/Nu_7	Nu_4/Nu_7
5	1.00	1.000	1.000	1.025	1.007
60	1.00	0.982	1.004	1.005	1.003
75	1.00	0.804	1.752	0.904	0.919
5	0.75	1.000	1.000	1.025	1.007
60	0.75	1.001	1.003	1.012	1.004
75	0.75	0.924	1.331	0.971	0.939
5	0.50	0.998	0.998	1.025	1.007
60	0.50	1.068	1.003	1.037	1.006
75	0.50	1.223	0.997	1.082	0.986
5	0.25	0.989	0.994	1.024	1.007
60	0.25	1.054	1.001	1.044	1.008
5	0.00	0.967	0.987	1.017	1.005
60	0.00	0.974	0.991	1.012	1.004

symmetric body. The same rationale used above for the cylinder, regarding the choice of the G_1 function, applies to the sphere as well. However, the authors found no experimental pressure distribution for the flow of power-law fluids over the sphere, so one for Newtonian fluids [12] was used. In the polynomial of Fage [12], which is shown below with the other G functions used for the sphere, an adverse pressure gradient is provided beginning at 74°.

$$G_1 = 1.5\phi - 0.4371\phi^3 + 0.1481\phi^5 - 0.0423\phi^7$$

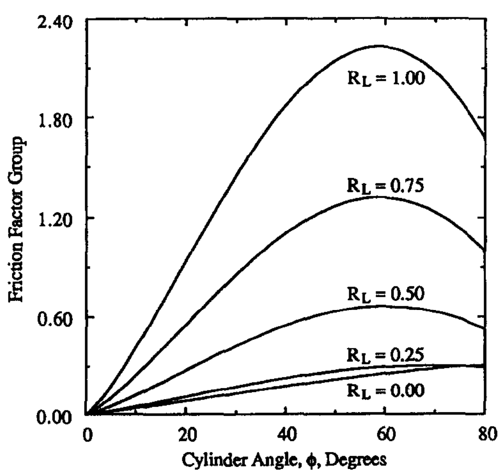

FIG. 4. Local friction factor group curves for the horizontal circular cylinder; $n = 1.6$, $Pr = 100$.

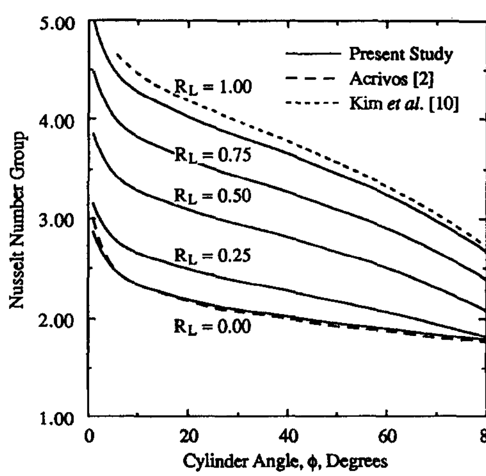

FIG. 5. Local Nusselt number group curves for the horizontal circular cylinder and comparison with refs. [2, 10]; $n = 1.6$, $Pr = 100$.

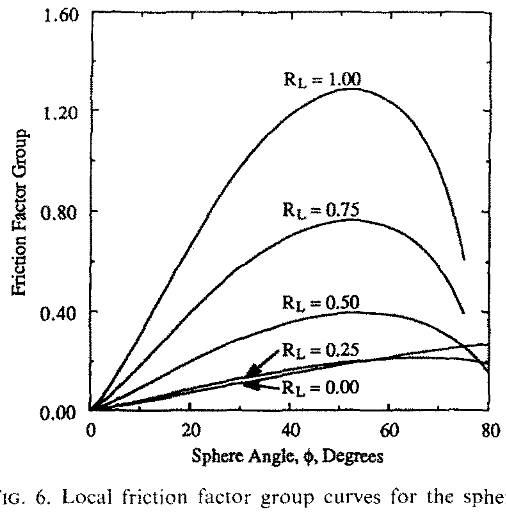

FIG. 6. Local friction factor group curves for the sphere; $n = 1.6$, $Pr = 100$.

$$G_2 = \sqrt{(2(1-\cos\phi))} \quad G_5 = \sin\phi. \tag{46}$$

Table 5 shows the relative convergence of the Merk–Chao series for the sphere. For the majority of the results, the convergence may be regarded as very good. As mentioned above, for flows with forced convection dominating, the series seem to need more terms for high sphere angles, which again precludes an accurate prediction of the separation point.

Figures 6 and 7, respectively, show the friction factor and Nusselt number group curves. Again, the Nusselt number curve for the natural convection extreme is compared with Acrivos [2]. The agreement is within 2.5% for the entire curve, except for $\phi < 10^\circ$.

5. CONCLUDING REMARKS

The Merk–Chao series solution method has been used to analyze the laminar, aiding, mixed-convective, boundary-layer flow of power-law fluids past isothermal, two-dimensional or axisymmetric bodies of arbitrary contour. The specific flow situation information is conveyed implicitly to the ordinary differential equation sets governing the universal functions through three mixed-convection parameters. Tabulated results for combinations of these three parameters for various n, Pr combinations have been presented elsewhere [10], and the results of the application of the method to the flat plate, the horizontal cylinder and the sphere have been presented herein.

For the limiting cases of pure-forced and pure-natural convection, the friction factor and Nusselt number group agreement with the literature is good. Since the solutions are expanded about the local similarity solution, the extension herein to mixed-convection is expected to have produced accurate results as well. For proper Reynolds number flows, the technique constitutes a general, simple and relatively computationally inexpensive alternative to the solution of the unreduced governing conservation equations for predicting the complicated transport phenomena occurring in mixed convection to power-law fluids. The restrictions that have historically limited many boundary-layer solutions for power-law fluid flows, namely a dominant convection mode, a specific geometry or high Pr, do not apply to the present work.

It is believed that the work in this paper and ref. [10] mark the first solutions presented from applying the Merk–Chao series technique to analyze mixed convection to power-law fluids and, for the limiting case of pure-natural convection, the first results for $n > 1$. Also, it seems that this study constitutes the first application of Merk–Chao series for computing the heat transfer in the forced flow of power-law fluids. The importance of the energy parameter (Λ_E)-related terms in the series has, to the best of the authors' knowledge, been investigated for the first time. The authors feel that velocity and temperature fields from this analysis form a good basis for predicting the mass transfer in power-law fluids for heterogeneous surface reactions.

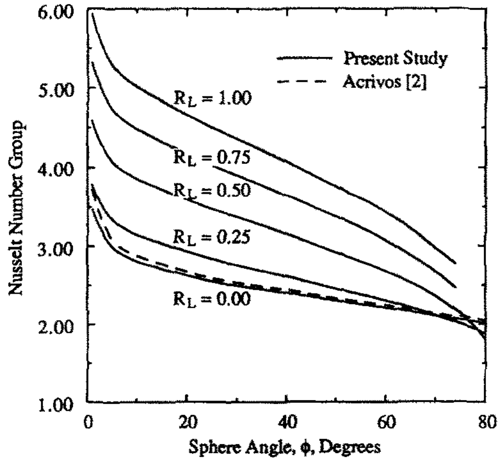

FIG. 7. Local Nusselt number group curves for the sphere and comparison with ref. [2]; $n = 1.6$, $Pr = 100$.

REFERENCES

1. A. M. Acrivos, M. J. Shah and E. E. Petersen, Momentum and heat transfer in laminar boundary-layer flows of non-Newtonian fluids past external surfaces, *A.I.Ch.E. Jl* **6**, 312–317 (1960).
2. A. M. Acrivos, A theoretical analysis of laminar natural convection heat transfer to non-Newtonian fluids, *A.I.Ch.E. Jl* **6**, 584–590 (1960).
3. H. J. Merk, Rapid calculations for boundary-layer transfer using wedge solutions and asymptotic expansions, *J. Fluid Mech.* **5**, 460–480 (1959).
4. D. Meksyn, *New Methods in Laminar Boundary-Layer Theory*, Chaps. 6, 7 and 9. Pergamon Press, Oxford (1961).
5. W. B. Bush, Local similarity expansions of the boundary-layer equations, *AIAA J.* **2**, 1857–1858 (1964).
6. B. T. Chao and R. O. Fagbenle, On Merk's method of calculating boundary layer transfer, *Int. J. Heat Mass Transfer* **17**, 223–240 (1974).
7. M. R. Cameron, D. R. Jeng and K. J. De Witt, Mixed forced and natural convection from two-dimensional or

axisymmetric bodies of arbitrary contour, *Int. J. Heat Mass Transfer* **34,** 582–587 (1991).
8. H. W. Kim, D. R. Jeng and K. J. De Witt, Momentum and heat transfer in power-law fluid flow over two-dimensional or axisymmetrical bodies, *Int. J. Heat Mass Transfer* **26,** 245–259 (1983).
9. T. A. Chang, D. R. Jeng and K. J. De Witt, Natural convection to power-law fluids from two-dimensional or axisymmetric bodies of arbitrary contour, *Int. J. Heat Mass Transfer* **31,** 615–624 (1988).
10. D. L. Meissner, An analysis of the mixed forced and natural convective flow of a power-law fluid over an isothermal, two-dimensional or axisymmetric body of arbitrary contour, Part I of Master's Thesis, University of Toledo, Toledo, Ohio (1992).
11. M. J. Shah, E. E. Petersen and A. M. Acrivos, Heat transfer from a cylinder to a power-law non-Newtonian fluid, *A.I.Ch.E. Jl* **8,** 542–549 (1960).
12. F. M. White, *Viscous Fluid Flow* (2nd Edn), p. 298. McGraw-Hill, New York (1991).